

## Article

# Improvement of the Carbocatalytic Degradation of Pharmaceuticals in Water by the Use of Ultrasound Waves

Carolina Quimbaya-Nañez<sup>1</sup>, Efraím A. Serna-Galvis<sup>1,2</sup>, Javier Silva-Agredo<sup>1</sup>,  
Inés García-Rubio<sup>3</sup>, Ricardo A. Torres-Palma<sup>1,\*</sup> and Yenny P. Ávila-Torres<sup>1,\*</sup>

<sup>1</sup> Grupo de Investigación en Remediación Ambiental y Biocatálisis (GIRAB), Instituto de Química, Facultad de Ciencias Exactas y Naturales, Universidad de Antioquia UdeA, Calle 70 No. 52-21, Medellín 050014, Colombia; carolina.quimbaya@udea.edu.co (C.Q.-Ñ.); efrain.serna@udea.edu.co (E.A.S.-G.); javier.silva@udea.edu.co (J.S.-A.)

<sup>2</sup> Catalizadores y Adsorbentes (CATALAD), Instituto de Química, Facultad de Ciencias Exactas y Naturales, Universidad de Antioquia UdeA, Calle 70 No. 52-21, Medellín 050014, Colombia

<sup>3</sup> Department of Condensed Matter Physics, Faculty of Sciences, University of Zaragoza, 50009 Zaragoza, Spain; inesgr@unizar.es

\* Correspondence: ricardo.torres@udea.edu.co (R.A.T.-P.); yenny.avila@udea.edu.co (Y.P.Á.-T.)

**Abstract:** A carbonaceous material obtained from wood wastes (SW-Mn) was initially used for the removal of pharmaceuticals in water by a carbocatalytic system. The SW-Mn material adsorbed only 41% of the diclofenac (DCF) and 3% of the valsartan (VAL). Interestingly, SW-Mn activated peroxymonosulfate (PMS) and presented a significant increase in the removal rate of DCF, surpassing 90%, while VAL achieved a 24% removal rate at 20 min of treatment. The carbonaceous material was not effective in activating peroxydisulfate or hydrogen peroxide. Nevertheless, the addition of ultrasound waves at 40 kHz to the carbocatalytic system (SW-Mn +PMS) significantly enhanced VAL degradation, exhibiting a high synergy index (4.98). The routes of the degradation were determined using scavengers, and XPS and EPR analyses, evidencing the main action of singlet oxygen in both carbocatalytic and sonocarbocatalytic systems. It is important to note that radicals also participated in the sonocarbocatalytic process, albeit with a minor contribution. The reuse of SW-Mn was tested during various cycles, showing up to a 39.2% VAL degradation rate after the third consecutive reuse. Moreover, the sonocarbocatalytic system was applied to a sample of irrigation crop water spiked with VAL. The treatment induced a partial elimination of the pollutant due to some interfering effects of the matrix components.

**Keywords:** carbocatalytic; pharmaceuticals elimination; sonocarbocatalytic; synergistic effects



**Citation:** Quimbaya-Nañez, C.; Serna-Galvis, E.A.; Silva-Agredo, J.; García-Rubio, I.; Torres-Palma, R.A.; Ávila-Torres, Y.P. Improvement of the Carbocatalytic Degradation of Pharmaceuticals in Water by the Use of Ultrasound Waves. *Water* **2023**, *15*, 3679. <https://doi.org/10.3390/w15203679>

Academic Editor: Lucas Santos-Juanes

Received: 8 September 2023

Revised: 11 October 2023

Accepted: 16 October 2023

Published: 20 October 2023



**Copyright:** © 2023 by the authors. Licensee MDPI, Basel, Switzerland. This article is an open access article distributed under the terms and conditions of the Creative Commons Attribution (CC BY) license (<https://creativecommons.org/licenses/by/4.0/>).

## 1. Introduction

Pharmaceuticals are chemical substances with therapeutic applications that can alter the physiologic processes of diverse living forms [1,2]. Pharmaceuticals are not totally metabolized in human and animal bodies. Therefore, portions of these compounds are excreted through urine or sweat. In many cases, pharmaceuticals reach the sewage systems with a subsequent input into the environmental water [3]. Moreover, the inadequate disposal of unused or expired pharmaceutical products promotes their improper discharge into the environment [4]. However, in most countries worldwide, the input of pharmaceuticals into the environment is not adequately regulated [3,5,6]. Therefore, the influence of pharmaceuticals on aquatic ecosystems is not fully understood [7].

Currently, there is a growing concern in the scientific community about the adverse environmental effects of widely used pharmaceuticals, such as antihypertensives or analgesics. For example, the antihypertensive valsartan can induce the growth inhibition of *Desmodesmus subspicatus* (algae), having an EC<sub>50</sub> value of ~115 mg L<sup>-1</sup> [8]. Additionally, the analgesic diclofenac has strong toxic effects on aquatic animals, birds, and plants. Diclofenac

is toxic to organisms in water even at very low environmental concentrations (e.g.,  $\text{ng L}^{-1}$  levels). This analgesic may also induce negative ecological risk to non-targeted organisms due to its biomagnification in the food chain [9]. Therefore, strategies to eliminate these pharmaceuticals and avoid their negative environmental impact must be applied.

It is important to mention that conventional wastewater treatment plants (WWTPs) are not designed for the degradation of pharmaceuticals [10]. Generally, WWTPs have a pre-treatment stage that can consist of roughing or desanding systems, and aerobic and anaerobic biological treatments using microorganisms in a controlled environment. In some cases, WWTPs can have a tertiary treatment for polishing the effluent [11–13]. The conventional processes of WWTPs are not efficient for the elimination of pharmaceuticals because these compounds are recalcitrant to the available treatments therein and they are also bio-accumulable [10,14,15]. Hence, the investigation of alternative treatments for the elimination of compounds recalcitrant to the conventional processes is necessary.

Alternative treatments, such as advanced oxidation processes (AOPs), have been sought to deal with refractory substances in water. AOPs involve the degradation of pollutants by the action of reactive oxygen species (ROS, e.g., hydroxyl radical or singlet oxygen) [16]. The carbocatalytic process, which uses carbonaceous materials as catalysts to produce ROS, is considered an AOP. This process has attracted attention in recent years due to the potential for carbon-based materials from agro-industrial wastes to be utilized [17–19]. Moreover, carbon-based material can be easily prepared from renewable sources such as biomass. The obtained materials are environmentally friendly and sustainable alternatives to traditional catalysts [20,21]. In the carbocatalytic processes, biochar or activated carbon is employed for the activation of oxidizing agents such as peroxymonosulfate (PMS) [19]. The carbocatalytic process can degrade pollutants by non-radical and radical pathways [22,23]. On the other hand, hybrid processes can increase the efficiency of the catalytic process by combining ultrasound and carbocatalysis. This combination generates a new process called sonocarbocatalysis [24–30].

There are some previous works on sonocarbocatalysis [24–30]. For instance, Cherifi et al. (2018) investigated PMS activation using reduced graphene oxide (rGO) combined with ultrasound for the removal of rhodamine B, bisphenol A, and tetracycline. The pollutants reached complete degradation and a high rate of total organic carbon removal (85%). Based on the results, a mechanism was proposed in which rGO activates PMS under ultrasound, leading to the generation of  $\text{HO}^\bullet$  and  $\text{SO}_4^{\bullet-}$  [30]. Additionally, Liu et al. (2022) evaluated the removal of humic acids in the biochar/ peroxydisulfate and ultrasound system. That investigation presented a high removal rate of humic acids (HAs). In fact, pollutant removal rates were achieved of 92.5% for the biochar/ peroxydisulfate/ultrasound system, 84.0% for the biochar and persulfate process, 52.0% for sole biochar, 50.0% for combined biochar/ultrasound, 10.0% for combined persulfate/ultrasonic, 4.0% for sole ultrasonic, and 1.0% for sole persulfate systems [24]. Despite the good results, these previous works have not presented information about the effect of ultrasound frequency on the sonocarbocatalytic process, nor compared the activation of diverse peroxides (PMS, persulfate, and hydrogen peroxide) in their systems. Likewise, they do not mainly involve non-radical pathways for pollutant elimination, nor are theoretical calculations included in such literature.

This work provides new information about the sonocarbocatalytic process, evaluating the effects of ultrasound frequency and peroxide type. Also, we supported the discussion of the interaction between peroxide and carbocatalyst on computational calculations. In this sense, a carbonaceous material synthesized from problematic wastes (SW-Mn) was used as a catalyst. This material was used in carbocatalysis and sonocarbocatalysis to deal with the merging concern of two contaminants of a pharmaceutical nature (i.e., valsartan and diclofenac). Herein, the degradation enhancement by combining carbocatalysis with ultrasound waves was evaluated. The effects of pollutant type, ultrasound frequency, peroxide type, pH, and matrix complexity (using actual irrigation crop water) were investigated. Additionally, the reuse cycles of the carbocatalyst were considered. Furthermore, the main

degrading species involved in the processes were established using EPR and XPS analyses, plus scavenging tests. Finally, the synergy of the combination of processes was determined.

## 2. Materials and Methods

### 2.1. Reagents

Sodium diclofenac ( $C_{14}H_{11}NCl_2O_2 \cdot Na$ , Table S1 in the Supplementary Materials) was obtained from Research Pharmaceuticals. Valsartan ( $C_{24}H_{29}N_5O_3$ , Table S1) was supplied by Abbott Operations, Abbott Park, Chicago, IL, USA. Acetonitrile ( $C_2H_3N$ ), formic acid ( $CH_2O_2$ ), hydrochloric acid (HCl), hydrogen peroxide ( $H_2O_2$ ), manganese carbonate ( $MnCO_3$ ), methanol ( $C_2H_6O$ ), sulfuric acid ( $H_2SO_4$ ), sodium azide ( $NaN_3$ ), sodium hydroxide (NaOH), sulfuric acid ( $H_2SO_4$ ), sodium sulfide ( $Na_2SO_3$ ), and p-benzoquinone ( $C_6H_4O_2$ ) were provided by Merck, Rahway, NJ, USA. Oxone ( $KHSO_5 \cdot 0.5 KHSO_4 \cdot 0.5 K_2SO_4$ ), which is the source of potassium peroxymonosulfate (PMS,  $KHSO_5$ ), was acquired from Sigma-Aldrich, Burlington, MA, USA. Sodium peroxydisulfate (PDS,  $Na_2S_2O_8$ ) was obtained from Fisher Scientific, Waltham, MA, USA.

### 2.2. Methods

#### 2.2.1. Carbonaceous Material Preparation

Sawdust waste (RW) was collected from a local wood industry in Medellin, Colombia. The sawdust sample (40 g) was subjected to pyrolysis at 500 °C for 2 h within a Mueller & Kempel muffle furnace, obtaining a biochar (SW). SW was impregnated with  $MnCO_3$  for 12 h with a mass ratio of 1:3 (SW: metal ion). Then, it was heated to 800 °C for 1 h, obtaining the SW-Mn material. The SW-Mn was washed with 0.01 M HCl until nearly neutral in pH (6.5–7.5). Finally, it was dried at 105 °C for 24 h. It is important to mention that the pyrolysis process was performed within a nitrogen atmosphere, with a flow rate of 124.8 mL per minute.

#### 2.2.2. Reaction Systems

The carbocatalysis experiments were performed in a batch-type reactor using an ultraturax stirrer system, containing 350 mL of sample to be treated. Meanwhile, in the sonocarbocatalytic process, a Meinhardt Ultrasound reactor was utilized, containing a volume of 350 mL of diclofenac (DCF) or valsartan (VAL) solution at a concentration of 0.0306 mM with 0.5 mM of peroxide and 0.5 g L<sup>-1</sup> of the catalyst (SW-Mn). The catalyst and PMS concentrations were chosen according to previous work by our research team [16,31,32].

For the ultrasound-assisted carbocatalysis treatment, a power density of 62.0 W L<sup>-1</sup> and a frequency of 40 kHz or 375 kHz were applied. Moreover, the experiments were carried out for 30 min. The influence of the peroxide type ( $H_2O_2$ , PDS, and PMS) and the initial solution pH (3.0, 5.8, and 9.0) were evaluated. Additionally, the reusability for three consecutive cycles and the feasibility of the system in a real matrix (irrigation crop water) doped with the selected pollutants were tested. The identification of ROS participants in the process was estimated using scavengers. *Tert*-butanol and methanol were used to quench  $HO^\bullet$  and  $SO_4^{\bullet-}$ , respectively [21,33]. Sodium azide and *p*-benzoquinone were utilized to determine the role of  $O_2^{\bullet-}$  and  $^1O_2$  species, respectively, in the removal of the pollutants [34,35]. Moreover, electron paramagnetic resonance spectroscopy (EPR) was carried out. Additionally, the synergy of carbocatalysis and sonocarbocatalysis was calculated using Equations (1) and (2) [36]:

$$S = \frac{\%R_{carbocatalysis}}{\%R_{Oxidant} + \%R_{SW-Mn}} \quad (1)$$

$$S = \frac{\%R_{carbocatalysis-US}}{\%R_{US} + \%R_{Oxidant} + \%R_{SW-Mn}} \quad (2)$$

where %R represent the percentages of elimination for each system indicated by the subscript. In turn, S means the synergy and its value equal to or higher than 1 denote additive

and synergistic effects, respectively. However, values of *S* lower than 1 indicate an antagonistic effect.

### 2.3. Analyses

#### 2.3.1. Chromatographic Analyses

The evolution of pollutants was analyzed using a UHPLC Thermo-Scientific (Waltham, MA, USA) Dionex UltiMate 3000 instrument equipped with an Acclaim™ 120 RP C18 column (5 μm, 4.6 × 150 mM). For the chromatographic analysis of DCF, a mixture of acetonitrile and formic acid in a ratio of 30:70 (% *v/v*) and a flow of 0.5 mL min<sup>-1</sup> was used, and the detection was set at 230 nm. Meanwhile, for chromatographic analysis of VAL, acetonitrile (44% *v/v*), formic acid (46% *v/v*, 10 mM, and pH 3.0), and methanol (10% *v/v*) were used as the mobile phase at a flow of 0.6 mL min<sup>-1</sup> and the detection was set at 254 nm.

#### 2.3.2. Electron Paramagnetic Resonance Spectroscopy (EPR)

EPR was performed using a Bruker (Billerica, MA, USA) ASAP-2010. The EPR instrument was operated at a center field of 3514.8 G, a sweep width of 100.0 G, and a power of 10 mW with a sweeping time of 30 s. DEPMPO (5-(diethoxyphosphoryl)-5-methyl-1-pyrroline-N-oxide) was used as a spin-trapping agent to identify O<sub>2</sub><sup>•-</sup>, while TEMP (2,2,6,6-tetramethylpiperidine) was employed to detect the presence of the hydroxyl radical and <sup>1</sup>O<sub>2</sub>.

#### 2.3.3. SW-Mn Characterization

The Brunauer–Emmett–Teller (BET) analyses were used to determine the surface area and pore information; a surface area and pore size analyzer, Quatachrome (Boynton Beach, FL, USA) NOVA 1200e, was employed. Surface functional groups were determined using Fourier-transformed infrared spectroscopy (FT-IR). The analysis was carried out using a Bruker (Billerica, MA USA) Tensor 27 spectrometer with an MCT (Mercury–Cadmium–Telluride) detector, using the diamond lens attenuated total reflectance (ATR) accessory. X-ray photoelectron spectroscopy (XPS) results were collected on an EnviroESCA SPECS instrument (Berlin, Germany). An aluminum X-ray source and a two-channel collector were used. The X-ray anode was operated at 12 keV and 250 W, and the vacuum was maintained at or below 5 × 10<sup>-7</sup> Torr. The pass energy for survey-wide scans was 89.45 eV, while 20 eV was used for narrow scan tests. The narrow scan spectra were employed for the determination of Mn (MnO, MnO<sub>2</sub>). Data were analyzed using Multi Pak Spectrum-ESCA. The XPS binding energies for the Mn 2p<sub>3/2</sub>, C 1s O 1s, and Si 2p core levels of samples were calculated, and assignments of photoemission signals corresponding to the chemical compounds were performed. Elemental composition was determined using the atomic sensitivity factor (ASF) of the orbital. The Horiba Yvon Jobin dispersive micro-Raman spectrophotometer was utilized to determine structural defects. Dynamic light scattering (DLS) analyses, using a Malvern (Malvern, UK) Zetasizer Pro analyzer, was performed to determine the particle size. The zero-charge point (PZC) was determined by the pH-metric method. Firstly, a mass of 0.20 g of the material was weighed and added into 50 mL of a 0.1 M NaCl solution. The method was carried out at pH values between 3.0 and 11.0. Finally, the PZC was determined by plotting ΔpH values versus initial pH [37].

#### 2.3.4. Theoretical Calculations

Computational modeling was performed to gain insights into the interaction of PMS, PDS or H<sub>2</sub>O<sub>2</sub> with SW-Mn. The structural geometries were optimized using the BIOVIA Material Studio 2017 with universal and Compass II force field. The simulation software version 2017 (Dassault Systems Biovia Corp, 2017) BIOVIA Forcite was utilized in this study, as reported by Shankar et al. [38]. To build the surface model, the elemental analysis ratios and potential of zero charge were employed. The activated carbon structure was chosen with O-containing groups including carboxyl, hydroxyl and ketone to obtain the corresponding functionalized surface model.

### 3. Results

The results are presented in five subsections. First, a brief characterization of the carbocatalyst is presented. Then, the carbocatalytic process is described for the removal of pollutants. Afterward, the sonocarbocatalytic system is studied. Herein, the effects of ultrasound frequency, oxidant type, and pH are evaluated. Subsequently, the participation of reactive oxygen species (ROS) during the carbocatalysis and sonocarbocatalysis processes is established using scavengers, and EPR and XPS analyses. At the end of the results section, SW-Mn reuse cycles and the matrix effects are presented.

#### 3.1. Brief Characterization of the SW-Mn Material

The SW-Mn material exhibited a higher specific surface area ( $S_{\text{BET}}$ ) compared to its precursors (i.e., RW and SW). The  $S_{\text{BET}}$  values were  $4.1 \pm 0.22$ ,  $10.2 \pm 0.76$ , and  $103.7 \pm 5.6 \text{ m}^2 \text{ g}^{-1}$ , corresponding to RW, SW, and SW-Mn, respectively. Within the FT-IR spectra for SW-Mn, two peaks were observed at  $481 \text{ cm}^{-1}$  and  $604 \text{ cm}^{-1}$ , which correspond to Mn–O vibrations [39–41]. Likewise, in the XPS analysis, after the deconvolution of the Mn  $2p^{3/2}$  orbital, the presence of the Mn–O species was confirmed. Moreover, the presence of oxygen-containing bonds such as those formed in alcohol and silanol groups was evidenced [42–44].

#### 3.2. Effect of Pollutant

The tests of the adsorption and carbocatalytic capabilities of SW-Mn were carried out to remove the two considered pollutants (DCF and VAL). Figure 1 shows the removal of the pollutants by these two processes. Figure 1 also presents the direct oxidation of the two pharmaceuticals by PMS acting alone. It can be noted that PMS induced partial oxidation of the pollutants (~15% for each), and the adsorption of DCF by SW-Mn (~40%) was higher than that of VAL. At the same time, the carbocatalytic process was more efficient at degrading DCF than VAL.

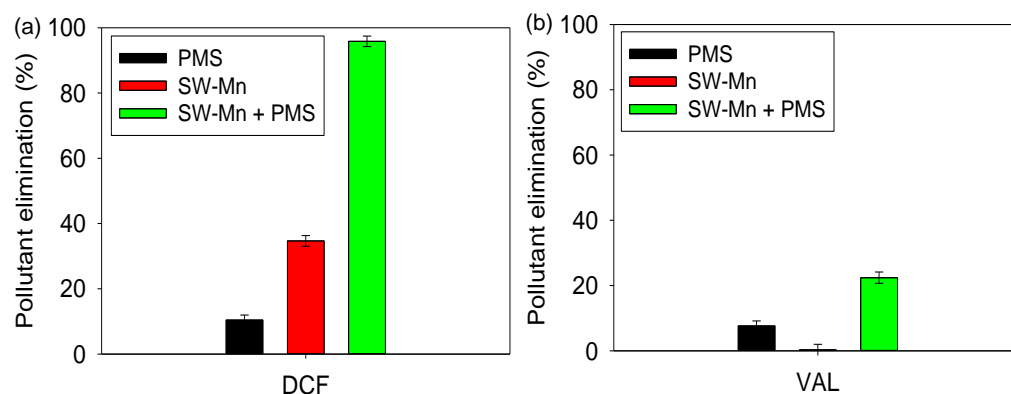


**Figure 1.** Elimination of the target pollutants by PMS, adsorption, and carbocatalysis, after 30 min of treatment: (a) DCF; and (b) VAL. Conditions: pollutant = 0.0306 mM; PMS = 0.5 mM; SW-Mn = 0.5 g L<sup>-1</sup>; V = 350 mL; matrix = distilled water; and initial pH = 5.8.

#### 3.3. Sonocarbocatalysis Process

Considering that VAL exhibited a lower degradation rate than DCF by both adsorption and carbocatalytic processes (Figure 1), the antihypertensive was submitted to sonocarbocatalysis. The effects of ultrasound frequency, peroxide type, and pH on the process were assessed and are detailed in the following sections.

##### 3.3.1. Effect of Ultrasound Frequency

Figure 2 presents the treatment of VAL by the sonocarbocatalytic system, evaluating two different frequencies (40 and 375 kHz). Additionally, control experiments of ultrasound (US) alone and carbocatalysis are included in Figure 2. It is remarkable that at high

frequency the US alone can degrade the target pollutant [45]. This process can achieve a similar degradation rate to that obtained by the carbocatalytic or sonocarbocatalytic systems. Interestingly, at 40 kHz, VAL elimination was strongly augmented through the combination of carbocatalysis with the ultrasound waves.

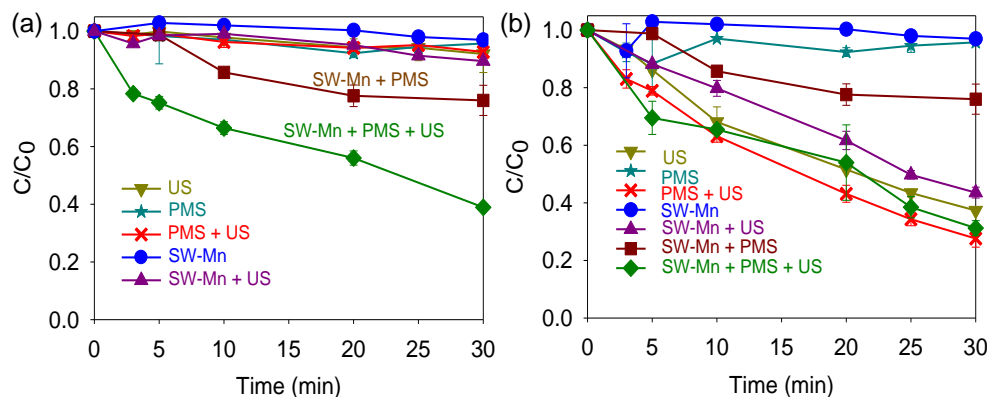


**Figure 2.** Effect of the ultrasound frequency on the sonocarbocatalytic treatment: (a) 40 kHz; and (b) 375 kHz. Conditions: pollutant = 0.0306 mM; PMS = 0.5 mM; SW-Mn = 0.5 g L<sup>-1</sup>; V = 350 mL; matrix = distilled water; and initial pH = 5.8.

### 3.3.2. Effect of the Peroxide Type (H<sub>2</sub>O<sub>2</sub>, PDS, and PMS)

It has been reported that, in addition to PMS, carbon-based catalysts can also activate other inorganic peroxides such as PDS and H<sub>2</sub>O<sub>2</sub> [46–49]. These oxidants contain a peroxide bond (O–O) and they are precursors of ROS and are useful for water treatment [50,51]. Therefore, the capability of SW-Mn to activate these diverse peroxides was evaluated, considering the sonocarbocatalysis process herein. Figure 3 presents the corresponding results. It was observed that the degrading performance for the tested system followed the order H<sub>2</sub>O<sub>2</sub> < PDS < PMS.

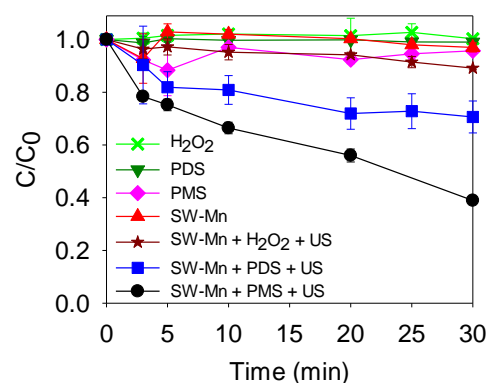


**Figure 3.** Effect of the peroxide type (H<sub>2</sub>O<sub>2</sub>, PDS, and PMS) on the elimination of VAL by sonocarbocatalysis. Conditions: pollutant = 0.0306 mM; PMS = 0.5 mM; SW-Mn = 0.5 g L<sup>-1</sup>; V = 350 mL; matrix = distilled water; frequency = 40 kHz; and initial pH = 5.8.

### 3.3.3. Effect of the pH

The pH plays an important role in the interaction between the pollutants and catalyst [52,53]. Therefore, the performance of the sonocarbocatalysis process, at three different initial pH values—acid (pH 3.0), natural (pH 5.8), and alkaline (pH 9.0)—was evaluated (Figure 4). It was found that sonocarbocatalytic degradation of VAL was not influenced by the initial pH of the solution.

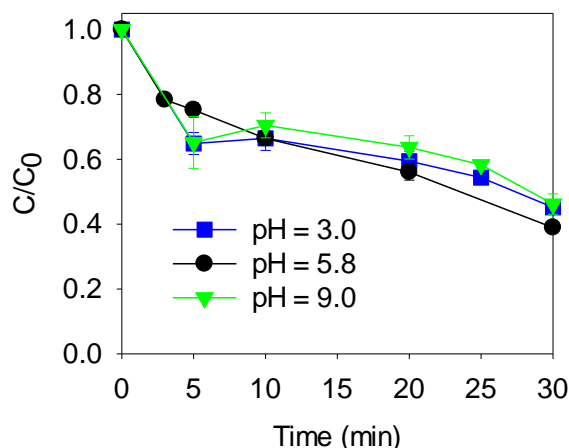


**Figure 4.** Effect of the initial pH (3.0, 5.8, and 9.0) on the elimination of VAL by sonocarbocatalysis. Conditions: pollutant = 0.0306 mM; PMS = 0.5 mM; SW-Mn = 0.5 g L<sup>-1</sup>; V = 350 mL; matrix = distilled water; frequency = 40 kHz; and initial pH = 5.8.

### 3.4. Identification of ROS and Reaction Mechanism during the Carbocatalytic and Sonocarbocatalytic Treatments

#### 3.4.1. Role of the Reactive Oxygen Species (ROS) in the Processes

The participation of ROS in the degradation of pollutants, using SW-Mn + PMS and SW-Mn + PMS + US, was examined by adding quenching agents (Figure 5). For radicals such as HO<sup>•</sup> and SO<sub>4</sub><sup>•-</sup>, methanol (MeOH) and *tert*-butanol (TBA) were used as scavengers [33]. On the other hand, benzoquinone (BQ) and sodium azide (NaN<sub>3</sub>) were utilized as scavengers of O<sub>2</sub><sup>•-</sup> and <sup>1</sup>O<sub>2</sub>, respectively [34,35]. The results in Figure 5 show a significant inhibition of VAL degradation rate in the presence of BQ and NaN<sub>3</sub>.

To complement the scavenging experiments, EPR analyses using TEMP (which traps singlet oxygen) and DEPMPO (to detect both superoxide and hydroxyl radicals produced by systems [54]) were performed. Figure 6 presents the results of the EPR tests.

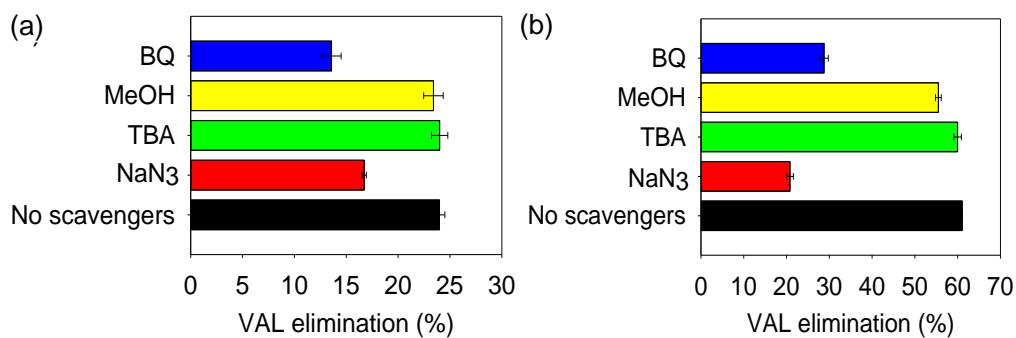
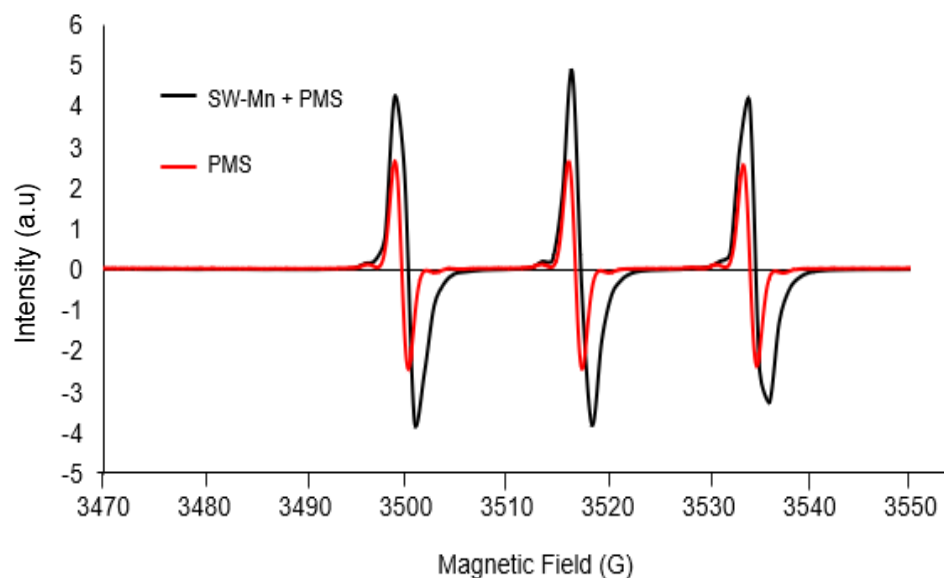
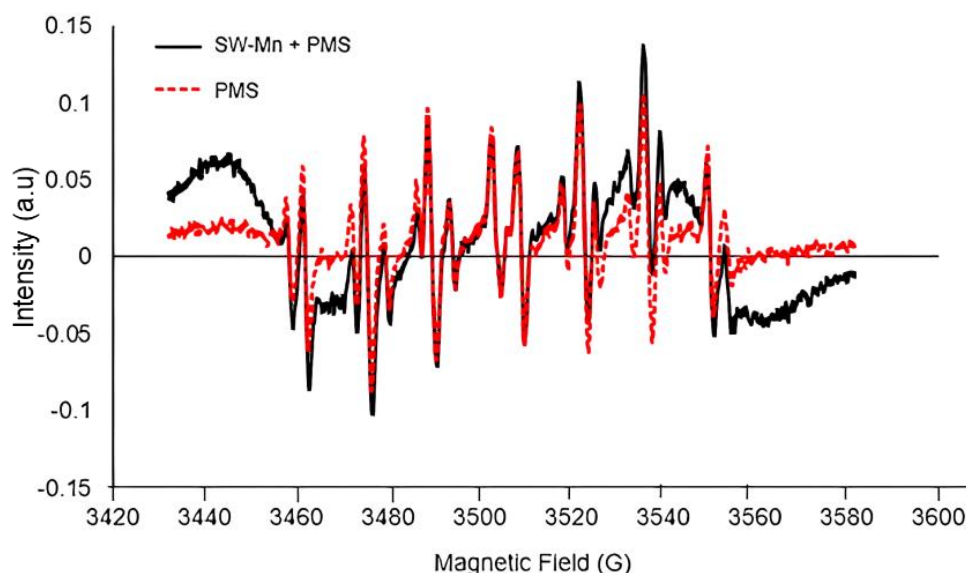


**Figure 5.** Identification of ROS after 30 min of treatment. VAL elimination (%) by (a) carbocatalysis, and (b) sonocarbocatalysis. Condition: pollutant = 0.0306 mM; PMS = 0.5 mM; SW-Mn = 0.5 g L<sup>-1</sup>; V = 350 mL; matrix = distilled water; frequency = 40 kHz; V = 350 mL; scavengers = 3 mM; and pH initial = 5.8 at 30 min.



(a)



(b)

**Figure 6.** EPR results for the interaction of SW-Mn with PMS: (a) participation of singlet oxygen; (b) participation of hydroxyl radical and superoxide.

### 3.4.2. Role of Manganese in the Processes

In the literature, it is reported that manganese oxides can oxidize organic pollutants [55–57]. As our carbocatalyst contains MnO, it is important to determine the role of Mn species in the sonocarbocatalytic process. Thus, manganese species before and after treatment were analyzed using XPS (Figure 7 and Table 1) [58,59]. The deconvolution of the Mn  $2p^{3/2}$  orbital indicated the presence of MnO in SW-Mn even after treatment corresponding to the third cycle of reuse.

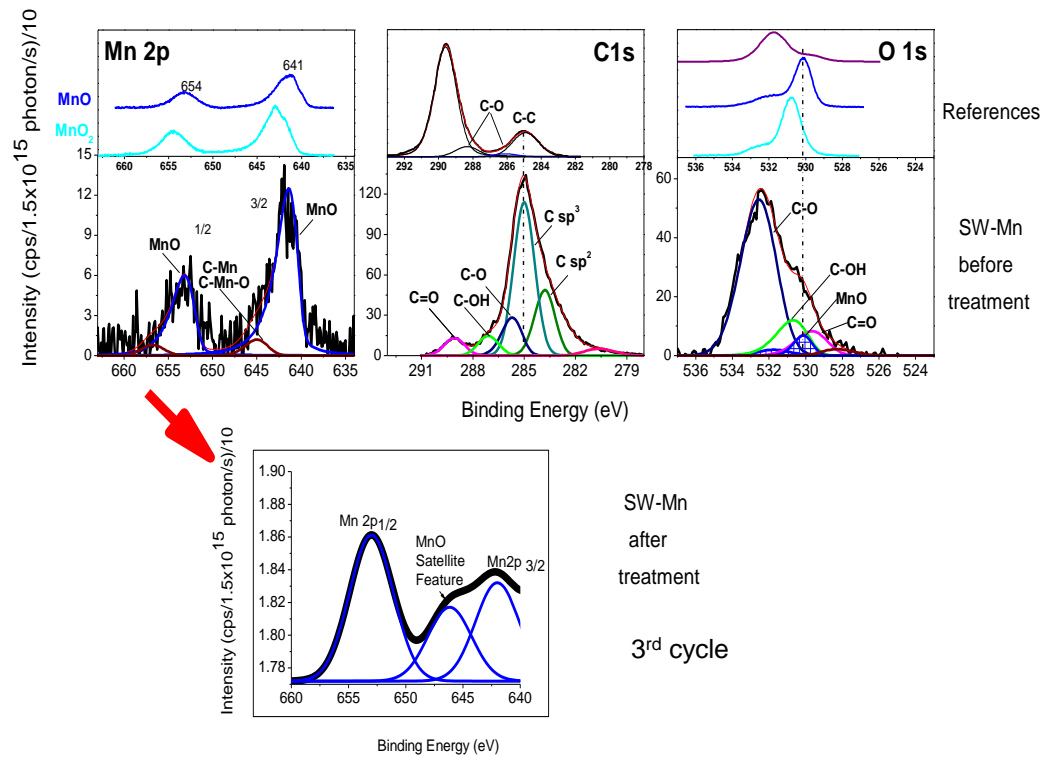


**Figure 7.** XPS spectra for SW-Mn before treatment and after the third cycle of treatment in sonocarbocatalysis. Red arrow represents a zoom in of the orbital Mn 2p in the SW-Mn material after the 3rd cycle of reuse.

### 3.5. Reuse of the Carbocatalyst and Effect of Water Matrix upon Sonocarbocatalysis

The reuse of the catalyst is another important criterion for the practical exploration of the catalytic performance because this provides information about the deactivation or poisoning of catalysts [60]. Hence, three reuse cycles for the adsorption, carbocatalysis, and sonocarbocatalysis processes were evaluated (Figure 8). The material has no significant adsorption of VAL at any cycle. Moreover, it can be noted that the degradation of the antihypertensive under the carbocatalytic and sonocarbocatalytic systems is stabilized after the first reuse cycle.

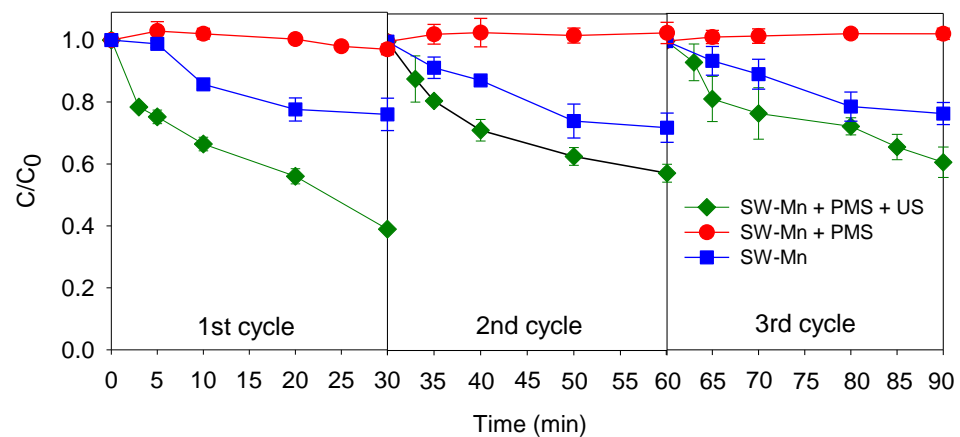


**Figure 8.** Reuse cycles for pollutant elimination. Conditions: pollutant = 0.0306 mM; PMS = 0.5 mM; SW-Mn = 0.5 g L<sup>-1</sup>; V = 350 mL; matrix = distilled water; frequency = 40 kHz; and initial pH = 5.8.

**Table 1.** XPS binding energies for the Mn 2p<sub>3/2</sub>, C 1s, O 1s, and Si 2p core levels of samples and assignment of photoemission signals corresponding to the chemical compounds. Elemental composition using the atomic sensitivity factor (ASF) of each orbital used.

Sample (Chem %)*	Mn 2p <sub>3/2</sub>		C 1s										O 1s		Si 2p	
	MnO	MnO <sub>2</sub>	Mn-C-O Mn-C	CH-CH Sp2	CH-CH Sp3	C-O	C-OH	Binding Energy (eV)					MnO sat	MnO <sub>2</sub> sat	C-Mn-O C-Mn	Si-O
								C=O	C-Mn-O C-Mn	O-C	O=C	OH-C				
C-Mn	641.40	---	645.00	283.79	285.00	285.70	287.10	289.08	282.69 280.63	532.55	529.65	530.68	530.13 531.74	---	528.30 ---	102.70
%	(91.5)	---	(8.5)	(19.3)	(46.2)	(11.1)	(5.8)	(5.2)	(9.5) (3.0)	(67.8)	(9.3)	(13.6)	(6.9)	---	(2.5)	(100)
SW-Mn before	641.40	642.80	645.00	283.79	285.00	285.64	287.10	289.08	282.69 280.20	532.66	529.65	530.55	530.13 531.74	530.78 532.48	527.60 525.60	102.70
%	(91.5)	(0)	(8.5)	(8.1)	(40.1)	(29.4)	(4.1)	(3.0)	(8.8) (6.4)	(47.2)	(18.4)	(11.4)	(14.4)	0	(7.9) (0.6)	(100)
SW-Mn after	641.40	642.80	645.00	283.79	285.00	285.70	287.10	289.08	282.69 ---	532.45	529.65	530.50	530.13 531.74	530.13 531.74	528.30 ---	102.70
%	(96.5)	(0)	(3.5)	(10.7)	(53.1)	(21.0)	(5.1)	(3.5)	(6.6)	(52.7)	(14.0)	(15.8)	(10.7)	(0)	(4.7)	(100)
MnO MnO <sub>2</sub>	641.40	542.80											530.13 531.74	530.78 532.48		
Sample	Mn		C				O					Si				
	Elemental composition (%) **															
C-Mn	4.3		76.1				18.7					1.0				
SW-Mn before%	9.8		62.7				25.7					1.8				
SW-Mn after%	8.4		64.7				24.6					2.3				

Note: \* Chemical percentage of group segments. Percentages of Mn oxides include core level Mn 2p and satellite shake-up peaks. \*\* Elemental composition used quantified XPS peaks of ASF at Mn 2p = 1.645, C 1s = 0.314, O 1s = 0.733 and Si 2p = 0.368.

On the other hand, some investigations have shown that the matrices of water modify the generation of ROS in the oxidation processes [61]. Additionally, substances such as nitrate ions ( $\text{NO}_3^-$ ), bicarbonate ions ( $\text{HCO}_3^-$ , associated with alkalinity), chloride ions ( $\text{Cl}^-$ ), and natural organic matter (NOM) are very common in real matrices [62]. Therefore, to obtain information about the matrix effect on VAL degradation in an actual matrix, a sample of real irrigation crop water spiked with the pollutant (Table 2) was treated by sonocarbocatalysis.

**Table 2.** Main characteristics of the irrigation crop water.

Parameters	Average Value
pH	7.5
Conductivity ( $\mu\text{S cm}^{-1}$ )	770
TOC ( $\text{mg L}^{-1}$ )	27.6
COD ( $\text{mg L}^{-1}$ )	54.4
Chlorides ( $\text{mg L}^{-1}$ )	68.5
Alkalinity ( $\text{mg L}^{-1}$ )	84.7

Figure 9 compares the removal rates of VAL in distilled water (DW) and in the real matrix by the SW-Mn + PMS + US system. The results show that in the complex matrix, the pollutant degradation was lower compared to DW.

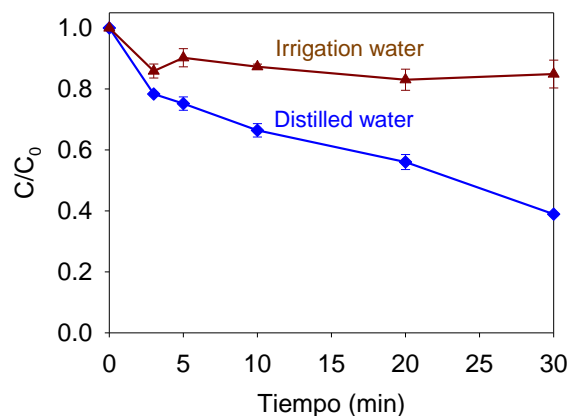


**Figure 9.** Elimination of VAL by sonocarbocatalysis in both distilled water and irrigation water. Conditions: pollutant = 0.0306 mM; catalyst = 0.5  $\text{g L}^{-1}$ ; PMS = 0.5 mM; density power = 62.0  $\text{W L}^{-1}$ ; frequency = 40 kHz; V = 350 mL; pH initial of distilled water = 5.8; and pH initial of irrigation water = 7.5.

## 4. Discussion

### 4.1. Adsorption and Carbocatalytic Processes

As mentioned above, the capability of the SW-Mn material to absorb DCF and VAL was initially tested. Figure 1 shows that SW-Mn resulted in 41.3% and 3.3% removal rates for DCF and VAL, respectively. According to Table 3, the specific surface area ( $S_{\text{BET}}$ ) of the SW-Mn decreased from  $103.7 \pm 5.6 \text{ m}^2 \text{ g}^{-1}$  to  $83.9 \text{ m}^2 \text{ g}^{-1}$  and  $96.8 \text{ m}^2 \text{ g}^{-1}$  after the adsorption treatment of DCF and VAL, respectively. The results confirm that DCF has a higher interaction with the material than VAL. The chemical structures of the two pharmaceuticals and the characteristics of the SW-Mn material should be considered to explain the differences in the adsorption results.

**Table 3.** Textural characterization of SW-Mn before and after the adsorption, carbocatalysis, and sonocarbocatalysis processes.

Process	$S_{\text{BET}}$ ( $\text{m}^2 \text{g}^{-1}$ )	$V_{\mu\text{P}}$ ( $\text{cm}^3 \text{g}^{-1}$ )	$V_{\text{MP}}$ ( $\text{cm}^3 \text{g}^{-1}$ )	$V_{\text{TP}}$ ( $\text{cm}^3 \text{g}^{-1}$ )	$D_{\text{AP}}$ (mm)
DCF					
Before	$103.7 \pm 5.6$	0.075	0.007	0.082	3.51
Adsorption	$83.9 \pm 4.3$	0.064	0.01	0.074	3.53
Carbocatalysis	$53.2 \pm 8.2$	0.045	0.007	0.052	3.91
VAL					
Before	$103.7 \pm 5.6$	0.075	0.007	0.082	3.51
Adsorption	$96.8 \pm 9.4$	0.075	0.007	0.078	3.22
Carbocatalysis	$68.9 \pm 6.6$	0.064	0.005	0.070	3.75
Sonocarbocatalysis	$55.5 \pm 8.3$	0.060	0.004	0.064	3.00

Note: Specific surface area ( $S_{\text{BET}}$ ) is calculated from the BET method (calculated in the linear  $P/P_0$  range from 0.05 to 0.22). The volume of the micropores ( $V_{\mu\text{P}}$ ) is from the DR method. The total pore volume ( $V_{\text{TP}}$ ). The volume of the mesopores ( $V_{\text{MP}}$ ) is from the difference between ( $V_{\mu\text{P}} - V_{\text{TP}}$ ). Average pore diameter ( $D_{\text{AP}}$ ).

DCF is a non-steroidal anti-inflammatory drug containing a phenylacetic acid and (2,6-dichlorophenyl)amino group at the 2-position (Figure S1a in the Supplementary Materials). Meanwhile, VAL is an antihypertensive that has a biphenyl-tetrazole and a 3-methyl butanoic acid linked to a pentanamide moiety (Figure S1b). It is relevant to consider that the zero-charge point (PZC) of the SW-Mn is 7.5. The aqueous samples at the beginning of the experiment have a pH value of 5.8. Therefore, under the experimental conditions, the solution  $\text{pH} < \text{PZC}$ , and the catalyst has positive surface charges. DCF has a  $\text{pK}_{\text{a}}$  of 4.0 (this is linked to the phenylacetic acid structure). Thus, under work conditions, the pollutant is negatively charged (Table S1, Figure S2a). Consequently, DCF adsorption is favored by electrostatic interactions. Moreover, the silanol and alcohol groups of SW-Mn could form hydrogen bonds with the carboxylate group in DCF and also with the N–H group of DCF. Also,  $\pi$ – $\pi$  interactions can occur between SW-Mn and the  $\text{sp}^2$  carbons at the aromatic rings in DCF [63]. In contrast to DCF, VAL ( $\text{pK}_{\text{a}1} = 3.9$  and  $\text{pK}_{\text{a}2} = 4.7$ ) had a double deprotonation (both carboxylic acid and tetrazole moieties, Table S1, Figure S2b). Although VAL is deprotonated and SW-Mn is protonated, and electrostatic interactions are possible, the adsorption is low. To explain this phenomenon, it is hypothesized that the presence of a few firstly adsorbed molecules of VAL (which is a big molecule) induces repulsion with other molecules of the same pollutant, thus hindering an effective adsorption process.

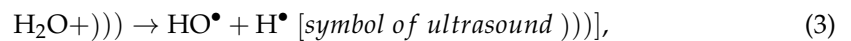
In addition to the adsorption of the pollutants on the carbonaceous material, the other control experiment (i.e., PMS alone) showed partial degradation of DCF and VAL (Figure 1). PMS can oxidize the amine or carboxyl acids on DCF, whereas the amide group on VAL can be cleaved by peroxydisulfate [64,65]. Additionally, the elimination of the pollutants by carbocatalysis (i.e., SW-Mn + PMS) was assessed. A higher removal rate of the pharmaceuticals was found compared to direct PMS oxidation and adsorption by SW-Mn (Figures 1 and S1). After 20 min of treatment, the synergy values for the carbocatalysis of DCF and VAL were 2.13 and 3.05, respectively. The synergy can be associated with the generation of ROS (see Section 4.3), produced by the interaction between the material and peroxydisulfate, which accelerates the removal of the pollutants. Also, it is important to mention that the results of DCF removal by the carbocatalytic process are comparable to those reported in other studies where catalysts with manganese were used to activate persulfates. For example, Wang et al. (2023) employed a biogenic manganese oxide to activate PMS and remove pollutants. The investigators reported that the contaminants reached high removal percentages (>80%) at 20 min of treatment, particularly for pollutants such as DCF (100%) [66]. Furthermore, Zhao et al. (2022) prepared and evaluated a material of  $\text{MnO}_2\text{-Bi}_2\text{O}_3$  to activate PMS for DCF removal. Using  $3.75 \text{ g L}^{-1}$  of the catalyst and  $0.125 \text{ g L}^{-1}$  of PMS, ~100% pollutant removal was reached [67].

Despite the synergy of the carbocatalytic system to degrade both pharmaceuticals, the removal rate of DCF was greater than 78%, while the removal rate of VAL reached 27%

(Figure 1). Therefore, a strategy to improve the elimination of VAL could be the combination of carbocatalysis with ultrasound waves. This is discussed in the following section.

#### 4.2. Sonocarbocatalysis Process

The effect of the ultrasound frequency during sonocarbocatalysis (SW-Mn + PMS + US) was tested, showing that the use of 40 kHz is more favorable than 375 kHz for this combination (Figure 2). At high frequency, the ultrasound system alone degraded ~60% of VAL after 30 min of treatment. This is because, at the higher tested frequency, the production of radicals is superior. The acoustic cavitation phenomenon (i.e., generation, growth, pulsation, and severe collapse of microbubbles) homolyses water molecules to produce radical species (Equation (3) [68]). Also, ultrasound waves can promote the cleavage of PMS (Equation (4) [53]). However, the combination of US at high frequency with SW-Mn + PMS was antagonistic. At 375 kHz, the wavelength of the ultrasound is small (~4 mM, [69]), and the solid particles of the carbocatalyst can affect the field of waves, thus limiting the direct action of the ultrasound system (Figure 2b).

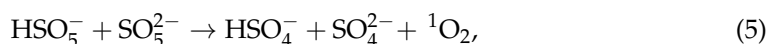


The removal rate of the pollutant using sonocarbocatalysis at 40 kHz is superior to carbocatalysis because the low ultrasound frequency predominantly induces physical effects (e.g., stirring and shock waves). These ultrasound waves promote disaggregation and break the solid material into smaller particles [70–72]. In fact, the average particle size decreased from ~800 nm to ~640 nm. Therefore, there is an increase in the number of active sites available on the catalyst for PMS activation. This phenomenon was also supported by the increase in the consumption of PMS in the presence of ultrasound (sonocarbocatalysis) in comparison with the carbocatalysis process. PMS is a hydrophilic molecule, and consequently, as the target pollutant, PMS is placed in the solution bulk [73]. Thus, stirring by ultrasound can favor the contact of VAL with PMS. Additionally, when the PMS is activated by ultrasound, the breaking of the O–O bonds can generate  $\text{HO}^\bullet$ , and  $\text{SO}_4^{\bullet-}$  (Equation (4)) in the solution bulk. The generated ROS are able to attack the pollutant, increasing the elimination of the contaminant [74], and leading to the synergistic degradation (S: 3.08) of VAL. According to these results, to perform the subsequent experiments in the sonocarbocatalytic system, the low ultrasonic frequency (i.e., 40 kHz) was utilized.

Furthermore, the influence of the peroxide type on VAL degradation by the sonocarbocatalytic process was also tested (Figure 3). The results showed that from the direct oxidizing action of  $\text{H}_2\text{O}_2$ , PDS, and PMS individually, the percentage of pollutant elimination was lower than ~11%. However, the elimination of the pollutants by the sonocarbocatalysis system with  $\text{H}_2\text{O}_2$  was similar to that observed by the adsorption of SW-Mn (Figure 3). Additionally, VAL elimination kinetics were greater for the sonocarbocatalysis process with PMS than with PDS (Figure 3). These findings indicate that SW-Mn was able to activate PMS, and, to a lower extent, PDS. However,  $\text{H}_2\text{O}_2$  was not activated. The asymmetric structure of the O–O bond in PMS can be activated more easily by a carbon-based catalyst than PDS or  $\text{H}_2\text{O}_2$  [75]. Our results are similar to those reported by Zhang et al., 2022, who evaluated a carbon-nanofiber-supported bimetallic catalyst (Co/Fe) for the treatment of ibuprofen. Their catalyst was used to activate PMS and PDS, finding that PMS is activated more efficiently than PDS [76]. Also, Xu et al., 2020, prepared and tested a nitrogen-doped biochar for the activation of  $\text{H}_2\text{O}_2$ , PDS, and PMS to degrade bisphenol A, reporting that the  $\text{H}_2\text{O}_2$  was not activated by the biochar, and the removal rate by PMS activation was higher than using PDS [77].

Once the effect of the oxidant was studied, the pH influence on the sonocarbocatalytic process was analyzed. As shown in Figure 4, VAL eliminations at pH 3.0, 5.8, and 9.0 were very similar. To interpret these results, we could consider the pKa values of PMS

and the pharmaceutical, and the PZC of SW-Mn. Since pH can modify the surface charges on SW-Mn (PZC value of 7.5), when the pH < PZC (e.g., at pH 3.0 or 5.8), the adsorption of VAL is expected to be lower due to intermolecular repulsion effects (as mentioned in Section 4.1). At pH 9.0, both VAL and the carbonaceous material are negatively charged, thus experiencing electrostatic repulsions. Therefore, VAL removal would be associated with catalytic action. Moreover, the PMS has a  $pK_{a1} < 0$  and  $pK_{a2} = 9.4$ . Hence, under alkaline conditions, PMS deprotonation and transformation into a less oxidative species ( $SO_5^{2-}$ ) can be induced, and at the same time singlet oxygen can be produced (Equation (5), the anion  $SO_5^{2-}$  initiates a nucleophilic reaction towards  $HSO_5^-$ ) [78]. VAL could also interact with weak oxidants such as a sulfur pentoxide anion or singlet oxygen. Furthermore, the pollutant elimination was not influenced by the working pH. These results suggest that the MnO on the SW-Mn material did not participate in VAL elimination (Figure 7). However, in further works, complementary analyses (e.g., new theoretical trials and adsorption tests at different pH values, plus comparisons of FT-IR results for the SW-Mn material before and after the interaction with VAL) could be performed to better clarify the role of pH in the VAL treatment.



### 4.3. Identification of ROS and Reaction Mechanism during the Carbocatalytic and Sonocarbocatalytic Treatment

#### 4.3.1. Role of the Reactive Oxygen Species in the Processes

The pollutant removal rates using the carbocatalytic and sonocarbocatalytic processes decreased when adding BQ (Figure 5a,b). The results suggest that  $O_2^{\bullet-}$  radical participated in VAL elimination. However, the limitation of using BQ as a scavenger of  $O_2^{\bullet-}$  must be considered as BQ can be absorbed by carbonaceous materials [79–81]. In addition, the inhibition of VAL degradation by the presence of  $NaN_3$  also suggests the participation of singlet oxygen in the degradation of the pharmaceutical. However, it must be considered that sodium azide can also directly react with PMS [82]. Meanwhile, the presence of MeOH and TBA did not inhibit the elimination of pollutants in the carbocatalysis process (i.e., there is no participation of radicals in the process). In contrast, only the MeOH slightly inhibited VAL removal by sonocarbocatalysis (Figure 5b). These results indicate low participation of the radical species in the sonocarbocatalytic process for degrading VAL.

To confirm the role of ROS on VAL degradation, EPR analyses were carried out (Figure 6). The interaction of SW-Mn + PMS/TEMP led to bigger signal intensities than PMS/TEMP (Figure 6a). The results evidenced the formation of singlet oxygen from the interaction between the carbonaceous material and peroxymonosulfate. Meanwhile, the trapping essays with DEPMPO exhibited very similar signals and intensities for SW-Mn + PMS/DEPMPO and PMS/DEPMPO (Figure 6b). These last results indicate a poor formation of hydroxyl radical and superoxide radical anions from the interaction between the carbonaceous material and peroxymonosulfate. Therefore, according to all the results presented above (using scavengers and EPR),  ${}^1O_2$  plays an important role in the degradation of VAL in the SW-Mn + PMS and SW-Mn + PMS + US systems. Meanwhile, the radicals have a lower participation during sonocarbocatalysis.

#### 4.3.2. Role of Manganese in the Processes

SW-Mn was subjected to further analysis using X-ray Photoelectron Spectroscopy (XPS). In Figure 7 and Table 1, two reference materials, MnO and  $MnO_2$ , were employed for comparison. Before and after the third cycle of reuse, the binding energy of Mn 2p<sub>3/2</sub> was determined to be 641.3 eV, while the binding energy of Mn 2p<sub>1/2</sub> was found to be 654 eV, corresponding to MnO. Additionally, a MnO satellite feature was observed at 646.2 eV, before and after three cycles of reuse. This observation indicates that manganese (II) does not participate in the redox catalytic process actively.

### 4.3.3. Understanding the Interaction between SW-Mn and PMS

Theoretical calculations for the interaction of the three peroxides with SW-Mn were carried out using BIOVIA Material Studio 2017 with universal and Compass II force fields (Figure 10). The results show that the SW-Mn + PMS system has a lower HOMO and LUMO pair than SW-Mn + PDS and SW-Mn + H<sub>2</sub>O<sub>2</sub>. This suggests that the interaction of SW-Mn with PMS is more favorable. Moreover, the Mn–O bonds in SW-Mn can form a new atomic configuration, which may favor the local formation of charged domains at the material surface (blue, pink, and yellow zones in Figure 10) and increase electrostatic repulsion between the material surface and anionic species. PDS is double negatively charged and PMS has a single negative charge, so lower HOMO–LUMO energies are observed for the SW-Mn + PMS system in Figure 10. For this reason, the interaction between peroxymonosulfate and the carbonaceous material is more favored.

In addition to the theoretical calculations and to better support the interaction of SW-Mn with PMS, the integrated intensity ratio of D-band versus G-band ( $I_D/I_G$ , obtained from the Raman spectra) was considered. This analysis provides valuable information about the defective degrees of the carbocatalyst. Defects are relevant in the activation of PMS using carbonaceous materials [83,84]. The SW-Mn material presents a high  $I_D/I_G$  value (1.40), with  $sp^2$  hybridization, which is useful for activating PMS. The structural defects can promote the generation of <sup>1</sup>O<sub>2</sub> (Equation (6)) [85,86], also explaining the high capability of SW-Mn to produce singlet oxygen.

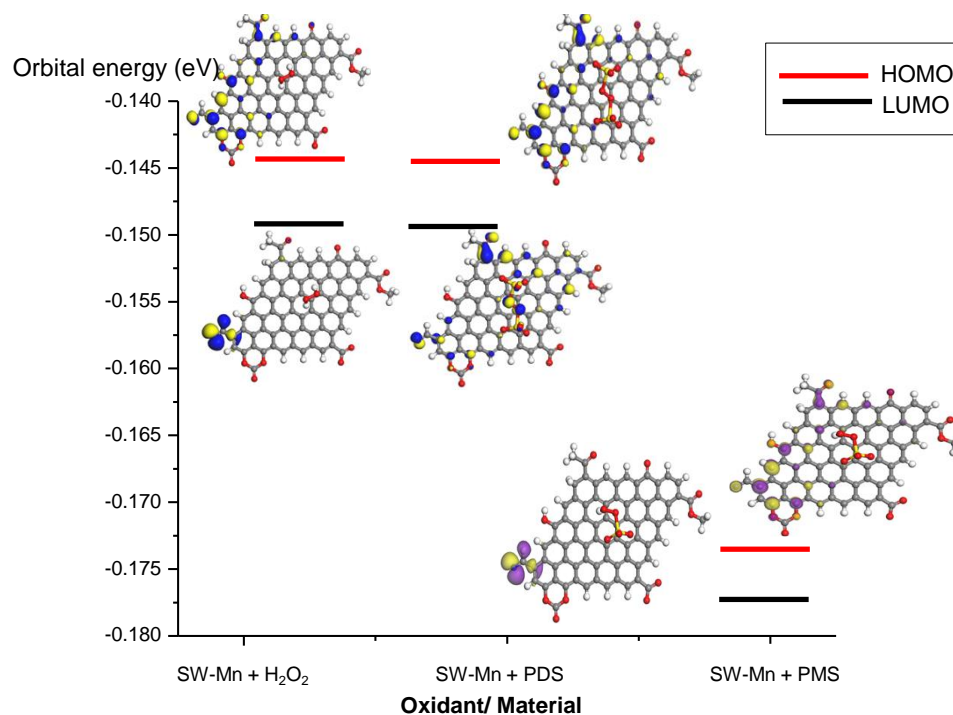


**Figure 10.** The optimized geometries and HOMO and LUMO energies for SW-Mn interacting with PMS, PDS, and H<sub>2</sub>O<sub>2</sub>, which were calculated using BIOVIA Material Studio 2017 with the universal and Compass II force fields. Red line represents the HOMO orbital energy and black line is the LUMO orbital energy. In the figure of the SW-Mn + Oxidant interactions, grey balls: carbon atoms white balls: hydrogen atoms, red balls: oxygen atoms, small yellow balls linked to the red ones: sulfur atoms; and blue-yellow and violet-blue lobules: the orbital lobules.

#### 4.4. Applications: Reuse and Effect of Water Matrix upon Sonocarbocatalysis

This section regards the reuse of the SW-Mn material to deal with VAL (Figure 8). VAL elimination by the SW-Mn + PMS + US and SW-Mn + PMS systems decreased from 61.1% to 39.2% and from 24.0% to 23.5% after the third cycle, respectively. It should be noted that the sonocarbocatalytic system is less affected than the carbocatalytic one, due to the effects promoted by the ultrasound. Table 2 shows the decrease in  $S_{\text{BET}}$  to  $96.8 \text{ m}^2 \text{ g}^{-1}$ ,  $68.9 \text{ m}^2 \text{ g}^{-1}$ , and  $55.5 \text{ m}^2 \text{ g}^{-1}$  for adsorption, carbocatalysis, and sonocarbocatalysis after first reuse, respectively. These results suggest that VAL adsorption or its degradation byproducts, and the SW-Mn modifications by the interaction with PMS during the processes, affected the material performance in the subsequent reuse cycles [60,87].

Furthermore, when comparing the elimination of VAL in distilled water (DW) and the real matrix, it was observed that the process is able to partially degrade the pollutant in a complex matrix. In fact, in DW, 60% of VAL was eliminated at 30 min, while only 15% of the pollutant was removed in the irrigation crop water (Figure 9). According to Table 2, natural organic matter is present in the complex matrix, which can interact with the singlet oxygen [88,89] formed in the sonocarbocatalytic system. Also, chloride or bicarbonate anions in the matrix can compete with VAL for the few radical species generated in the process [90–92]. Furthermore, some matrix components could be adsorbed on the SW-Mn surface, interfering with the PMS activation. As a consequence of all these factors, VAL elimination in the irrigation crop water is lower than in distilled water.

## 5. Conclusions

The SW-Mn material was a better adsorbent for DCF than for VAL due to more favorable interactions with the former contaminant. The carbonaceous material was able to activate PMS for the degradation of the pharmaceuticals, but PDS and  $\text{H}_2\text{O}_2$  were not activated. Indeed, theoretical and experimental analyses showed that the interactions between SW-Mn and PMS have low energy and promote the generation of degrading species. VAL degradation (SW-Mn + PMS) was improved by the addition of ultrasound waves of low frequency (i.e., 40 kHz). This kind of US promoted mechanical effects (e.g., the carbocatalyst particle disaggregation or better contact between reagents).

In the sonocarbocatalytic process (i.e., SW-Mn + PMS + US), according to the inhibition by scavengers and EPR analyses, the singlet oxygen was the main degrading agent, with a small participation of radical species. The sonocarbocatalytic degradation of VAL presented a good performance at a wide range of initial pH (pH 3–9). However, the SW-Mn exhibited low reusability in the processes for VAL elimination. Moreover, the pollutant removal rate by sonocarbocatalysis decreased in irrigation crop water compared to distilled water. This was because the components of the water matrix affected the degradation pathways during treatment.

**Supplementary Materials:** The following supporting information can be downloaded at: <https://www.mdpi.com/article/10.3390/w15203679/s1>, Figure S1: Chemical structure (a) Diclofenac, and (b) Valsartan; Figure S2: Structures of (a) Diclofenac and (b) Valsartan, according to their pKa values; Table S1: Characteristics of the pharmaceuticals; Supplementary references: [93–98].

**Author Contributions:** Conceptualization, E.A.S.-G., Y.P.Á.-T. and R.A.T.-P.; methodology, C.Q.-Ñ.; software, Y.P.Á.-T.; formal analysis, C.Q.-Ñ., E.A.S.-G., J.S.-A., I.G.-R., R.A.T.-P. and Y.P.Á.-T.; investigation, C.Q.-Ñ., E.A.S.-G. and Y.P.Á.-T.; resources, Y.P.Á.-T. and R.A.T.-P.; data curation, C.Q.-Ñ.; writing—original draft preparation, C.Q.-Ñ. and Y.P.Á.-T.; writing—review and editing, E.A.S.-G. and R.A.T.-P.; visualization, C.Q.-Ñ., E.A.S.-G. and Y.P.Á.-T.; supervision, Y.P.Á.-T. and R.A.T.-P.; project administration, Y.P.Á.-T. and R.A.T.-P.; funding acquisition, Y.P.Á.-T. and R.A.T.-P. All authors have read and agreed to the published version of the manuscript.

**Funding:** This research was funded by MINCIENCIAS COLOMBIA, grant number 1115-852-69594, Program to improve the quality of irrigation water through the elimination of emerging contaminants by advanced oxidation processes (PRO-CEC-AGUA).

**Data Availability Statement:** Data will be available via request to the authors.

**Conflicts of Interest:** The authors declare no conflict of interest.

## References

1. Dhawande, A.; Moon, S.; Kale, V.; Pethe, A.M.; Raut, N.A. Chapter 1—Pharmaceutical waste: An emerging threat to the ecosystem. In *360-Degree Waste Management*; Elsevier: Amsterdam, The Netherlands, 2023; Volume 2, pp. 3–37.
2. Glassman, P.M.; Muzykantov, V.R. Pharmacokinetic and pharmacodynamic properties of drug delivery systems. *J. Pharmacol. Exp. Ther.* **2019**, *370*, 570–580. [[CrossRef](#)] [[PubMed](#)]
3. Kumar, V.; Lakkaboyana, S.K.; Sharma, N.; Chakraborty, P.; Umesh, M.; Pasrija, R.; Thomas, J.; Kalebar, V.U.; Jayaraj, I.; Awasthi, M.K.; et al. A critical assessment of technical advances in pharmaceutical removal from wastewater—A critical review. *Case Stud. Chem. Environ. Eng.* **2023**, *8*, 100363. [[CrossRef](#)]
4. Insani, W.N.; Qonita, N.A.; Jannah, S.S.; Nuraliyah, N.M.; Supadmi, W.; Gatera, V.A.; Alfian, S.D.; Abdulah, R. Improper disposal practice of unused and expired pharmaceutical products in Indonesian households. *Heliyon* **2020**, *6*, 6–10. [[CrossRef](#)]
5. Ahmed, S.; Khan, F.S.A.; Mubarak, N.M.; Khalid, M.; Tan, Y.H.; Mazari, S.A.; Karri, R.R.; Abdullah, E.C. Emerging pollutants and their removal using visible-light responsive photocatalysis—A comprehensive review. *J. Environ. Chem. Eng.* **2021**, *9*, 106643. [[CrossRef](#)]
6. González-González, R.B.; Sharma, P.; Singh, S.P.; Américo-Pinheiro, J.H.P.; Parra-Saldívar, R.; Bilal, M.; Iqbal, H.M.N. Persistence, environmental hazards, and mitigation of pharmaceutically active residual contaminants from water matrices. *Sci. Total Environ.* **2022**, *821*, 153329. [[CrossRef](#)] [[PubMed](#)]
7. dos Santos, D.F.; Moreira, W.M.; de Araújo, T.P.; Bergamasco, R.; Ostroski, I.C.; de Barros, M.A.S.D. Non-conventional processes applied for the removal of pharmaceuticals compounds in waters: A review. *Process Saf. Environ. Prot.* **2022**, *167*, 527–542. [[CrossRef](#)]
8. Bayer, A.; Asner, R.; Schüssler, W.; Kopf, W.; Weiß, K.; Sengl, M.; Letzel, M. Behavior of sartans (antihypertensive drugs) in wastewater treatment plants, their occurrence and risk for the aquatic environment. *Environ. Sci. Pollut. Res.* **2014**, *21*, 10830–10839. [[CrossRef](#)]
9. Sathishkumar, P.; Meena, R.A.A.; Palanisami, T.; Ashokkumar, V.; Palvannan, T.; Gu, F.L. Occurrence, interactive effects and ecological risk of diclofenac in environmental compartments and biota—A review. *Sci. Total Environ.* **2020**, *698*, 134057. [[CrossRef](#)]
10. Botero-Coy, A.M.; Martínez-Pachón, D.; Boix, C.; Rincón, J.R.; Castillo, N.; Arias-Marín, L.P.; Manrique-Losada, L.; Torres-Palma, R.A.; Moncayo-Lasso, A.; Hernández, F. An investigation into the occurrence and removal of pharmaceuticals in colombian wastewater. *Sci. Total Environ.* **2018**, *62*, 842–853. [[CrossRef](#)]
11. Jasim, N.A. The design for wastewater treatment plant (WWTP) with GPS X modelling. *Cogent Eng.* **2020**, *7*, 1723782. [[CrossRef](#)]
12. Infrastructures, H. Design and construction of wastewater treatment plant (WWTP). Available online: [https://www.sice.com/sites/Sice/files/2016-10/ENV\\_EDAR\\_Construction\\_ENG\\_\(9\).pdf](https://www.sice.com/sites/Sice/files/2016-10/ENV_EDAR_Construction_ENG_(9).pdf) (accessed on 15 October 2023).
13. Englande, A.J.; Krenkel, P.A. Waste Water Treatment and Water Reclamation. In *Encyclopedia of Physical Science and Technology*; Elsevier: Amsterdam, The Netherlands, 2003; pp. 639–670.
14. Bwapwa, J.; Jaiyeola, A. Emerging Contaminants in Drinking Water and Wastewater, Effects on Environment and Remediation. *Int. J. Appl. Eng. Res.* **2019**, *14*, 539–546.
15. Arrubla, J.P.; Cubillos, J.A.; Ramírez, C.A.; Arredondo, J.A.; Arias, C.A.; Paredes, D. Pharmaceutical and personal care products in domestic wastewater and their removal in anaerobic treatment systems: Septic tank—Up flow anaerobic filter | Presencia de productos farmacéuticos y de cuidado personal en aguas residuales domésticas y su elim. *Ing. E Investig.* **2016**, *36*, 70–78. [[CrossRef](#)]
16. Serna-Galvis, E.A.; Martínez-Mena, Y.L.; Arboleda-Echavarría, J.; Hoyos-Ayala, D.A.; Echavarría-Isaza, A.; Torres-Palma, R.A. Zeolite 4A activates peroxymonosulfate toward the production of singlet oxygen for the selective degradation of organic pollutants. *Chem. Eng. Res. Des.* **2023**, *193*, 121–131. [[CrossRef](#)]
17. Ayanda, S. *Water Treatment Technologies: Principles, Applications, Successes and Limitations of Bioremediation, Membrane Bioreactor and the Advanced Oxidation Processes*; OMICS International: Hyderabad, India, 2017; ISBN 9781632780584.
18. Yu, J.; Zhu, Z.; Zhang, H.; Shen, X.; Qiu, Y.; Yin, D.; Wang, S. Persistent free radicals on N-doped hydrochar for degradation of endocrine disrupting compounds. *Chem. Eng. J.* **2020**, *398*, 125538. [[CrossRef](#)]
19. Gasim, M.F.; Veksha, A.; Lisak, G.; Low, S.C.; Hamidon, T.S.; Hussin, M.H.; Oh, W. Da Importance of carbon structure for nitrogen and sulfur co-doping to promote superior ciprofloxacin removal via peroxymonosulfate activation. *J. Colloid Interface Sci.* **2023**, *634*, 586–600. [[CrossRef](#)]
20. Lam, E.; Luong, J.H.T. Carbon materials as catalyst supports and catalysts in the transformation of biomass to fuels and chemicals. *ACS Catal.* **2014**, *4*, 3393–3410. [[CrossRef](#)]
21. Qu, S.; Yuan, Y.; Yang, X.; Xu, H.; Mohamed, A.K.; Zhang, J.; Zhao, C.; Liu, L.; Wang, B.; Wang, X.; et al. Carbon defects in biochar facilitated nitrogen doping: The significant role of pyridinic nitrogen in peroxymonosulfate activation and ciprofloxacin degradation. *Chem. Eng. J.* **2022**, *441*, 135864. [[CrossRef](#)]
22. Gao, Y.; Wang, Q.; Ji, G.; Li, A. Degradation of antibiotic pollutants by persulfate activated with various carbon materials. *Chem. Eng. J.* **2022**, *429*, 132387. [[CrossRef](#)]
23. Oh, W.D.; Lim, T.T. Design and application of heterogeneous catalysts as peroxydisulfate activator for organics removal: An overview. *Chem. Eng. J.* **2019**, *358*, 110–133. [[CrossRef](#)]

24. Liu, H.; Ye, M.; Ren, Z.; Lichtfouse, E.; Chen, Z. Towards synergistic combination of biochar/ultrasonic persulfate enhancing removal of natural humic acids from water. *J. Environ. Chem. Eng.* **2022**, *10*, 107809. [[CrossRef](#)]
25. Wang, X.; Wang, L.; Li, J.; Qiu, J.; Cai, C.; Zhang, H. Degradation of Acid Orange 7 by persulfate activated with zero valent iron in the presence of ultrasonic irradiation. *Sep. Purif. Technol.* **2014**, *122*, 41–46. [[CrossRef](#)]
26. Diao, Z.H.; Dong, F.X.; Yan, L.; Chen, Z.L.; Qian, W.; Kong, L.J.; Zhang, Z.W.; Zhang, T.; Tao, X.Q.; Du, J.J.; et al. Synergistic oxidation of Bisphenol A in a heterogeneous ultrasound-enhanced sludge biochar catalyst/persulfate process: Reactivity and mechanism. *J. Hazard. Mater.* **2020**, *384*, 121385. [[CrossRef](#)]
27. Cai, C.; Zhang, H.; Zhong, X.; Hou, L. Ultrasound enhanced heterogeneous activation of peroxymonosulfate by a bimetallic Fe-Co/SBA-15 catalyst for the degradation of Orange II in water. *J. Hazard. Mater.* **2015**, *283*, 70–79. [[CrossRef](#)] [[PubMed](#)]
28. Zhong, X.; Xiang, L.; Royer, S.; Valange, S.; Barrault, J.; Zhang, H. Degradation of C.I. Acid Orange 7 by heterogeneous Fenton oxidation in combination with ultrasonic irradiation. *J. Chem. Technol. Biotechnol.* **2011**, *86*, 970–977. [[CrossRef](#)]
29. Liu, F.; Yi, P.; Wang, X.; Gao, H.; Zhang, H. Degradation of Acid Orange 7 by an ultrasound/ZnO-GAC/persulfate process. *Sep. Purif. Technol.* **2018**, *194*, 181–187. [[CrossRef](#)]
30. Cherifi, Y.; Addad, A.; Vezin, H.; Barras, A.; Ouddane, B.; Chaouchi, A.; Szunerits, S.; Boukherroub, R. PMS activation using reduced graphene oxide under sonication: Efficient metal-free catalytic system for the degradation of rhodamine B, bisphenol A, and tetracycline. *Ultrason. Sonochem.* **2019**, *52*, 164–175. [[CrossRef](#)]
31. Sun, X.; Xu, D.; Dai, P.; Liu, X.; Tan, F.; Guo, Q. Efficient degradation of methyl orange in water via both radical and non-radical pathways using Fe-Co bimetal-doped MCM-41 as peroxymonosulfate activator. *Chem. Eng. J.* **2020**, *402*, 125881. [[CrossRef](#)]
32. Grisales-Cifuentes, C.M.; Serna-Galvis, E.A.; Acelas, N.; Porras, J.; Flórez, E.; Torres-Palma, R.A. Biochar from palm fiber wastes as an activator of different oxidants for the elimination of pharmaceuticals from diverse classes in aqueous samples. *J. Environ. Manage.* **2022**, *323*, 116148. [[CrossRef](#)]
33. Ademollo, N.; Spataro, F.; Rauseo, J.; Pescatore, T.; Fattorini, N.; Valsecchi, S.; Polesello, S.; Patrolecco, L. Occurrence, distribution and pollution pattern of legacy and emerging organic pollutants in surface water of the Kongsfjorden (Svalbard, Norway): Environmental contamination, seasonal trend and climate change. *Mar. Pollut. Bull.* **2021**, *163*, 111900. [[CrossRef](#)]
34. Zou, Y.; Li, W.; Yang, L.; Xiao, F.; An, G.; Wang, Y.; Wang, D. Activation of peroxymonosulfate by sp<sup>2</sup>-hybridized microalgae-derived carbon for ciprofloxacin degradation: Importance of pyrolysis temperature. *Chem. Eng. J.* **2019**, *370*, 1286–1297. [[CrossRef](#)]
35. Chen, X.; Oh, W.D.; Lim, T.T. Graphene-and CNTs-based carbocatalysts in persulfates activation: Material design and catalytic mechanisms. *Chem. Eng. J.* **2018**, *354*, 941–976. [[CrossRef](#)]
36. Torres-Palma, R.A.; Nieto, J.I.; Combet, E.; Pétrier, C.; Pulgarin, C. An innovative ultrasound, Fe<sup>2+</sup> and TiO<sub>2</sub> photoassisted process for bisphenol a mineralization. *Water Res.* **2010**, *44*, 2245–2252. [[CrossRef](#)] [[PubMed](#)]
37. Ahmad, R.; Ansari, K. Chemically treated Lawsonia inermis seeds powder (CTLISP): An eco-friendly adsorbent for the removal of brilliant green dye from aqueous solution. *Groundw. Sustain. Dev.* **2020**, *11*, 100417. [[CrossRef](#)]
38. Shankar, U.; Gogoi, R.; Sethi, S.K.; Verma, A. *Forcefields for Atomistic-Scale Simulations: Materials and Applications*; Springer: Berlin/Heidelberg, Germany, 2022; Volume 99, pp. 299–313. ISBN 9789811930928.
39. Wang, H.; Lu, Z.; Qian, D.; Li, Y.; Zhang, W. Single-crystal α-MnO<sub>2</sub> nanorods: Synthesis and electrochemical properties. *Nanotechnology* **2007**, *18*, 2–7. [[CrossRef](#)]
40. Racik, K.M.; Guruprasad, K.; Mahendiran, M.; Madhavan, J.; Maiyalagan, T.; Raj, M.V.A. Enhanced Electrochemical Performance of MnO<sub>2</sub>/NiO Nanocomposite for Supercapacitor Electrode with Excellent Cycling Stability. *J. Mater. Sci. Mater. Electron.* **2019**, *30*, 5222–5232. [[CrossRef](#)]
41. Tang, N.; Tian, X.; Yang, C.; Pi, Z.; Han, Q. Facile Synthesis of α-MnO<sub>2</sub> Nanorods for High-Performance Alkaline Batteries. *J. Phys. Chem. Solids* **2010**, *71*, 258–262. [[CrossRef](#)]
42. Motozuka, S.; Tagaya, M.; Hayashi, K.; Kameyama, T.; Oguri, H.; Xu, Z. Mechanochemical Surface Modification of Carbon Fibers Using a Simple Rubbing Method. *J. Compos. Mater.* **2017**, *51*, 3577–3584. [[CrossRef](#)]
43. Chen, Y.; Wang, H.; Dang, B.; Xiong, Y.; Yao, Q.; Wang, C.; Sun, Q.; Jin, C. Bio-Inspired Nacre-like Nanolignocellulose-Poly (Vinyl Alcohol)-TiO<sub>2</sub> Composite with Superior Mechanical and Photocatalytic Properties. *Sci. Rep.* **2017**, *7*, 1–9. [[CrossRef](#)]
44. Shircliff, R.A.; Stradins, P.; Moutinho, H.; Fennell, J.; Ghirardi, M.L.; Cowley, S.W.; Branz, H.M.; Martin, I.T. Angle-Resolved XPS Analysis and Characterization of Monolayer and Multilayer Silane Films for DNA Coupling to Silica. *Langmuir* **2013**, *29*, 4057–4067. [[CrossRef](#)]
45. Guateque-Londoño, J.F.; Serna-Galvis, E.A.; Ávila-Torres, Y.; Torres-Palma, R.A. Degradation of Losartan in Fresh Urine by Sonochemical and Photochemical Advanced Oxidation Processes. *Water* **2020**, *12*. [[CrossRef](#)]
46. Huang, D.; Zhang, Q.; Zhang, C.; Wang, R.; Deng, R.; Luo, H.; Li, T.; Li, J.; Chen, S.; Liu, C. Mn Doped Magnetic Biochar as Persulfate Activator for the Degradation of Tetracycline. *Chem. Eng. J.* **2020**, *391*, 123532. [[CrossRef](#)]
47. Ren, W.; Nie, G.; Zhou, P.; Zhang, H.; Duan, X.; Wang, S. The Intrinsic Nature of Persulfate Activation and N-Doping in Carbocatalysis. *Environ. Sci. Technol.* **2020**, *54*, 6438–6447. [[CrossRef](#)] [[PubMed](#)]
48. Yang, Y.; Zhang, X.; Ngo, H.H.; Guo, W.; Li, Z.; Wang, X.; Zhang, J.; Long, T. A New Spent Coffee Grounds Based Biochar-Persulfate Catalytic System for Enhancement of Urea Removal in Reclaimed Water for Ultrapure Water Production. *Chemosphere* **2022**, *288*, 132459. [[CrossRef](#)] [[PubMed](#)]
49. Forouzesh, M.; Ebadi, A.; Aghaeinejad-Meybodi, A. Degradation of Metronidazole Antibiotic in Aqueous Medium Using Activated Carbon as a Persulfate Activator. *Sep. Purif. Technol.* **2019**, *210*, 145–151. [[CrossRef](#)]

50. Ji, R.; Chen, J.; Liu, T.; Zhou, X.; Zhang, Y. Critical Review of Perovskites-Based Advanced Oxidation Processes for Wastewater Treatment: Operational Parameters, Reaction Mechanisms, and Prospects. *Chinese Chem. Lett.* **2022**, *33*, 643–652. [[CrossRef](#)]
51. Guateque-Londoño, J.F.; Serna-Galvis, E.A.; Silva-Agredo, J.; Ávila-Torres, Y.; Torres-Palma, R.A. Dataset on the Degradation of Losartan by TiO<sub>2</sub>-Photocatalysis and UVC/Persulfate Processes. *Data Br.* **2020**, *31*, 105692. [[CrossRef](#)]
52. Chen, X.-L.; Li, H.; Lai, L.; Zhang, Y.; Chen, Y.; Li, X.; Liu, B.; Wang, H. Peroxymonosulfate Activation Using MnFe<sub>2</sub>O<sub>4</sub> Modified Biochar for Organic Pollutants Degradation: Performance and Mechanisms. *Sep. Purif. Technol.* **2023**, *308*, 122886. [[CrossRef](#)]
53. Wang, J.; Wang, S. Activation of Persulfate (PS) and Peroxymonosulfate (PMS) and Application for the Degradation of Emerging Contaminants. *Chem. Eng. J.* **2018**, *334*, 1502–1517. [[CrossRef](#)]
54. Mojović, M.; Vuletić, M.; Bačić, G.G. Detection of Oxygen-Centered Radicals Using EPR Spin-Trap DEPMPO: The Effect of Oxygen. *Ann. N. Y. Acad. Sci.* **2005**, *1048*, 471–475. [[CrossRef](#)]
55. Zhang, H.; Huang, C.H. Oxidative Transformation of Fluoroquinolone Antibacterial Agents and Structurally Related Amines by Manganese Oxide. *Environ. Sci. Technol.* **2005**, *39*, 4474–4483. [[CrossRef](#)]
56. Yang, C.; Yang, Z.; Yang, K.; Yu, Z.; Zuo, Y.; Cheng, L.; Wang, Y.; Sun, H.; Yu, G.; Zhang, C.; et al. Periodate Activated by Different Crystalline Phases MnO<sub>2</sub> for Profound Oxidation Tetracycline Hydrochloride: Oxygen Vacancy-Dominated Active Pivots and Mechanism. *Sep. Purif. Technol.* **2022**, *301*, 122022. [[CrossRef](#)]
57. Gan, L.; Fang, X.; Xu, L.; Wang, L.; Wu, Y.; Dai, B.; He, W.; Shi, J. Boosted Activity of δ-MnO<sub>2</sub> by Kenaf Derived Carbon Fiber for High-Efficient Oxidative Degradation of Bisphenol A in Water. *Mater. Des.* **2021**, *203*, 1–11. [[CrossRef](#)]
58. Audi, A.A.; Sherwood, P.M.A. Valence-Band x-Ray Photoelectron Spectroscopic Studies of Manganese and Its Oxides Interpreted by Cluster and Band Structure Calculations. *Surf. Interface Anal.* **2002**, *33*, 274–282. [[CrossRef](#)]
59. Rosso, J.J.; Hochella, M.F. Natural Iron and Manganese Oxide Samples by XPS. *Surf. Sci. Spectra* **1996**, *4*, 253–265. [[CrossRef](#)]
60. Bartholomew, C.H. Mechanisms of Catalyst Deactivation. *Appl. Catal. A Gen.* **2001**, *212*, 17–60. [[CrossRef](#)]
61. Wang, J.; Wang, S. Effect of Inorganic Anions on the Performance of Advanced Oxidation Processes for Degradation of Organic Contaminants. *Chem. Eng. J.* **2021**, *411*, 128392. [[CrossRef](#)]
62. Hagan, G.B.; Minkah, R.; Yiran, G.A.B.; Dankyi, E. Assessing Groundwater Quality in Peri-Urban Accra, Ghana: Implications for Drinking and Irrigation Purposes. *Groundw. Sustain. Dev.* **2022**, *17*, 100761. [[CrossRef](#)]
63. Rigueto, C.V.T.; Rosseto, M.; Nazari, M.T.; Ostwald, B.E.P.; Alessandretti, L.; Manera, C.; Piccin, J.S.; Dettmer, A. Adsorption of Diclofenac Sodium by Composite Beads Prepared from Tannery Wastes-Derived Gelatin and Carbon Nanotubes. *J. Environ. Chem. Eng.* **2021**, *9*, 105030. [[CrossRef](#)]
64. Arvaniti, O.S.; Bairamis, F.; Konstantinou, I.; Mantzavinos, D.; Frontistis, Z. Degradation of Antihypertensive Drug Valsartan in Water Matrices by Heat and Heat/Ultrasound Activated Persulfate: Kinetics, Synergy Effect and Transformation Products. *Chem. Eng. J. Adv.* **2020**, *4*, 100062. [[CrossRef](#)]
65. Wang, S.; Wang, J. A Novel Strategy of Successive Non-Radical and Radical Process for Enhancing the Utilization Efficiency of Persulfate. *Chemosphere* **2020**, *245*, 125555. [[CrossRef](#)]
66. Wang, G.; Hambly, A.C.; Zhao, D.; Wang, G.; Tang, K.; Andersen, H.R. Peroxymonosulfate Activation by Suspended Biogenic Manganese Oxides for Polishing Micropollutants in Wastewater Effluent. *Sep. Purif. Technol.* **2023**, *306*, 122501. [[CrossRef](#)]
67. Zhao, W.; Duan, Z.; Zheng, Z.; Li, B. Efficient Diclofenac Removal by Superoxide Radical and Singlet Oxygen Generated in Surface Mn(II)/(III)/(IV) Cycle Dominated Peroxymonosulfate Activation System: Mechanism and Product Toxicity. *Chem. Eng. J.* **2022**, *433*, 133742. [[CrossRef](#)]
68. Camargo-Perea, A.L.; Serna-Galvis, E.A.; Lee, J.; Torres-Palma, R.A. Understanding the Effects of Mineral Water Matrix on Degradation of Several Pharmaceuticals by Ultrasound: Influence of Chemical Structure and Concentration of the Pollutants. *Ultrason. Sonochem.* **2021**, *73*, 105500. [[CrossRef](#)] [[PubMed](#)]
69. Lee, S.; Son, Y. Ultrasonics Sonochemistry Effects of Gas Saturation and Sparging on Sonochemical Oxidation Activity under Different Liquid Level and Volume Conditions in 300-KHz Sonoreactors: Zeroth- and First-Order Reaction Comparison Using KI Dosimetry and BPA Degradation. *Ultrason. Sonochem.* **2023**, *98*, 106521. [[CrossRef](#)] [[PubMed](#)]
70. Mohammadi, P.; Karami, N.; Zinatizadeh, A.A.; Falahi, F.; Aghamohammadi, N.; Almasi, A. Using High Frequency and Low-Intensity Ultrasound to Enhance Activated Sludge Characteristics. *Ultrason. Sonochem.* **2019**, *54*, 274–280. [[CrossRef](#)]
71. McKenzie, T.G.; Karimi, F.; Ashokkumar, M.; Qiao, G.G. Ultrasound and Sonochemistry for Radical Polymerization: Sound Synthesis. *Chem.-A Eur. J.* **2019**, *25*, 5372–5388. [[CrossRef](#)]
72. Ziylan-Yavaş, A.; Ince, N.H. Enhanced Photo-Degradation of Paracetamol on n-Platinum-Loaded TiO<sub>2</sub>: The Effect of Ultrasound and [Rad]OH/Hole Scavengers. *Chemosphere* **2016**, *162*, 324–332. [[CrossRef](#)]
73. Xu, L.; Wang, X.; Sun, Y.; Gong, H.; Guo, M.; Zhang, X.; Meng, L.; Gan, L. Mechanistic Study on the Combination of Ultrasound and Peroxymonosulfate for the Decomposition of Endocrine Disrupting Compounds. *Ultrason. Sonochem.* **2020**, *60*, 104749. [[CrossRef](#)]
74. Yin, R.; Guo, W.; Wang, H.; Du, J.; Zhou, X.; Wu, Q.; Zheng, H.; Chang, J.; Ren, N. Enhanced Peroxymonosulfate Activation for Sulfamethazine Degradation by Ultrasound Irradiation: Performances and Mechanisms. *Chem. Eng. J.* **2018**, *335*, 145–153. [[CrossRef](#)]
75. Gao, Y.; Zhu, Y.; Chen, Z.; Zeng, Q.; Hu, C. Insights into the Difference in Metal-Free Activation of Peroxymonosulfate and Peroxydisulfate. *Chem. Eng. J.* **2020**, *394*, 123936. [[CrossRef](#)]

76. Zhang, Y.; Yang, T.; Li, R.; Cao, X.; Kan, Y.; Wei, B.; Sun, X. Efficient Degradation of Ibuprofen by Co/Fe@CNFs Catalyst in the Presence of Peroxymonosulfate and Persulfate: Characterization, Performance, and Mechanism Comparison. *J. Taiwan Inst. Chem. Eng.* **2022**, *131*, 104161. [[CrossRef](#)]
77. Xu, L.; Wu, C.; Liu, P.; Bai, X.; Du, X.; Jin, P.; Yang, L.; Jin, X.; Shi, X.; Wang, Y. Peroxymonosulfate Activation by Nitrogen-Doped Biochar from Sawdust for the Efficient Degradation of Organic Pollutants. *Chem. Eng. J.* **2020**, *387*, 124065. [[CrossRef](#)]
78. Chen, Z.; Wang, L.; Xu, H.; Wen, Q. Efficient Heterogeneous Activation of Peroxymonosulfate by Modified CuFe<sub>2</sub>O<sub>4</sub> for Degradation of Tetrabromobisphenol A. *Chem. Eng. J.* **2020**, *389*. [[CrossRef](#)]
79. Nicomel, N.R.; Li, L.Y.; Mohamed, B.A.; Ramim, S.S. Adsorption of P-Benzoquinone at Low Concentrations from Aqueous Media Using Biosolid-Based Activated Carbon. *J. Environ. Manag.* **2022**, *316*, 115263. [[CrossRef](#)]
80. Li, G.; Zhu, W.; Zhu, L.; Chai, X. Effect of Pyrolytic Temperature on the Adsorptive Removal of P-Benzoquinone, Tetracycline, and Polyvinyl Alcohol by the Biochars from Sugarcane Bagasse. *Korean J. Chem. Eng.* **2016**, *33*, 2215–2221. [[CrossRef](#)]
81. Guoting, L.; Yanmin, F.; Xiaoqi, C.; Erming, L.; Qingtong, W.; Hao, Z. Efficient Adsorptive Removal of P-Benzoquinone by Lanthanum Modified Activated Carbon Fibre. *J. Environ. Eng.* **2016**, *10*, 1638–1644.
82. Lee, J.; Von Gunten, U.; Kim, J.H. Persulfate-Based Advanced Oxidation: Critical Assessment of Opportunities and Roadblocks. *Environ. Sci. Technol.* **2020**, *54*, 3064–3081. [[CrossRef](#)]
83. Yang, S.; Xu, S.; Tong, J.; Ding, D.; Wang, G.; Chen, R.; Jin, P.; Wang, X.C. Overlooked Role of Nitrogen Dopant in Carbon Catalysts for Peroxymonosulfate Activation: Intrinsic Defects or Extrinsic Defects? *Appl. Catal. B Environ.* **2021**, *295*, 120291. [[CrossRef](#)]
84. Tan, J.; Xu, C.; Zhang, X.; Huang, Y. MOFs-Derived Defect Carbon Encapsulated Magnetic Metallic Co Nanoparticles Capable of Efficiently Activating PMS to Rapidly Degrade Dyes. *Sep. Purif. Technol.* **2022**, *289*, 120812. [[CrossRef](#)]
85. Zhao, Y.; An, H.; Dong, G.; Feng, J.; Wei, T.; Ren, Y.; Ma, J. Oxygen Vacancies Induced Heterogeneous Catalysis of Peroxymonosulfate by Ni-Doped AgFeO<sub>2</sub> Materials: Evolution of Reactive Oxygen Species and Mechanism. *Chem. Eng. J.* **2020**, *388*, 124371. [[CrossRef](#)]
86. Kohantorabi, M.; Moussavi, G.; Giannakis, S. A Review of the Innovations in Metal- and Carbon-Based Catalysts Explored for Heterogeneous Peroxymonosulfate (PMS) Activation, with Focus on Radical vs. Non-Radical Degradation Pathways of Organic Contaminants. *Chem. Eng. J.* **2021**, *411*, 127957. [[CrossRef](#)]
87. Huang, W.; Xiao, S.; Zhong, H.; Yan, M.; Yang, X. Activation of Persulfates by Carbonaceous Materials: A Review. *Chem. Eng. J.* **2021**, *418*, 129297. [[CrossRef](#)]
88. Fang, Z.; Qi, J.; Xu, Y.; Liu, Y.; Qi, T.; Xing, L.; Dai, Q.; Wang, L. Promoted Generation of Singlet Oxygen by Hollow-Shell CoS/g-C<sub>3</sub>N<sub>4</sub> Catalyst for Sulfonamides Degradation. *Chem. Eng. J.* **2022**, *441*, 136051. [[CrossRef](#)]
89. Wu, S.; Yang, C.; Lin, Y.; Cheng, J.J. Efficient Degradation of Tetracycline by Singlet Oxygen-Dominated Peroxymonosulfate Activation with Magnetic Nitrogen-Doped Porous Carbon. *J. Environ. Sci. (China)* **2022**, *115*, 330–340. [[CrossRef](#)] [[PubMed](#)]
90. Li, Y.; Zheng, X.; Guo, Q.; Wang, X.; Zhang, L.; Zhu, W.; Luo, Y. Activation of Peroxymonosulfate by the CoFe/ZSM-5 for Efficient Sulfamethoxazole Degradation. *J. Environ. Chem. Eng.* **2022**, *10*, 107012. [[CrossRef](#)]
91. Liu, J.; Jiang, S.; Chen, D.; Dai, G.; Wei, D.; Shu, Y. Activation of Persulfate with Biochar for Degradation of Bisphenol A in Soil. *Chem. Eng. J.* **2020**, *381*, 122637. [[CrossRef](#)]
92. Guo, J.; Wen, X.; Yang, J.; Fan, T. Removal of Benzo(a)Pyrene in Polluted Aqueous Solution and Soil Using Persulfate Activated by Corn Straw Biochar. *J. Environ. Manage.* **2020**, *272*, 111058. [[CrossRef](#)]
93. Lara-Pérez, C.; Leyva, E.; Zermeño, B.; Osorio, I.; Montalvo, C.; Moctezuma, E. Photocatalytic degradation of diclofenac sodium salt: Adsorption and reaction kinetic studies. *Environ. Earth Sci.* **2020**, *79*, 1–13. [[CrossRef](#)]
94. Siddiqui, N.; Husain, A.; Chaudhry, L.; Alam, S.S.; Mitra, M.; Bhasin, P.S. Pharmacological and pharmaceutical profile of valsartan: A review. *J. Appl. Pharm. Sci.* **2011**, *1*, 12–19.
95. Kearney, P.M.; Whelton, M.; Reynolds, K.; Muntner, P.; Whelton, P.K.; He, J. Global burden of hypertension: Analysis of worldwide data. *Lancet* **2005**, *365*, 217–223. [[CrossRef](#)]
96. Nackiewicz, J.; Gąsowska-Bajger, B.; Kołodziej, L.; Poliwoda, A.; Pogoda-Mieszczak, K.; Skonieczna, M. Comparison of the degradation mechanisms of diclofenac in the presence of iron octacarboxyphthalocyanine and myeloperoxidase. *Spectrochim. Acta-Part A Mol. Biomol. Spectrosc.* **2023**, *287*. [[CrossRef](#)] [[PubMed](#)]
97. Shamsudin, M.S.; Azha, S.F.; Ismail, S. A review of diclofenac occurrences, toxicology, and potential adsorption of clay-based materials with surfactant modifier. *J. Environ. Chem. Eng.* **2022**, *10*, 107541. [[CrossRef](#)]
98. Vasantha Raman, N.; Gsell, A.S.; Voulgarellis, T.; van den Brink, N.W.; de Senerpont Domis, L.N. Moving beyond standard toxicological metrics: The effect of diclofenac on planktonic host-parasite interactions. *Aquat. Toxicol.* **2023**, *254*, 106370. [[CrossRef](#)] [[PubMed](#)]

**Disclaimer/Publisher's Note:** The statements, opinions and data contained in all publications are solely those of the individual author(s) and contributor(s) and not of MDPI and/or the editor(s). MDPI and/or the editor(s) disclaim responsibility for any injury to people or property resulting from any ideas, methods, instructions or products referred to in the content.